---

**Article:**
Roy, C, Winter, A, Ritter, JRR et al. (1 more author) (2017) On the improvement of SKS splitting measurements by the Simultaneous Inversion of Multiple Waveforms (SIMW). Geophysical Journal International, 208 (3). pp. 1508-1523. ISSN 0956-540X

https://doi.org/10.1093/gji/ggw470

---

Geophysical Journal International

*Geophys. J. Int.* (2017) **208,** 1508–1523
Advance Access publication 2016 December 23
GJI Seismology

doi: 10.1093/gji/ggw470

# On the improvement of SKS splitting measurements by the Simultaneous Inversion of Multiple Waveforms (SIMW)

C. Roy,[1,*] A. Winter,[1,†] J.R.R. Ritter[1] and J. Schweitzer[2,‡]

[1]*Karlsruhe Institute of Technology, Geophysical Institute, Germany. E-mail: corinna.roy@berkeley.edu*
[2]*NORSAR, Kjeller, Norway*

Accepted 2016 December 16. Received 2016 December 2; in original form 2016 February 28

## SUMMARY

The birefringence of core-refracted shear waves (e.g. SKS or SKKS) is often used to study seismic anisotropy in the Earth. However, depth resolution and multilayer anisotropy is generally poor for many regions on Earth. This is primarily due to SKS or SKKS phases that are not observable for different backazimuths either because of missing seismicity at the required distance range or because of a too low signal-to-noise ratio (SNR). We propose a new method called Simultaneous Inversion of Multiple Waveforms (SIMW), which allows the joint inversion of multiple core-refracted shear waves from different earthquakes within the same source region, observed by either the same seismic station or by a seismic network. The waveforms are concatenated into a combined signal, which is then inverted with the Silver & Chan method to determine the two splitting parameters: time delay $\delta t$, and fast polarization direction $\Phi$. We apply our method to recordings at the large aperture Norwegian NORSAR Array and the German Gräfenberg array (GRF). Our results demonstrate that SIMW allows a stable determination of splitting results for low-amplitude or noisy SKS signals. Splitting parameter uncertainties can be reduced and reliable results are obtained for both arrays. Moreover, new backazimuth directions can be explored, enabling a more accurate derivation of two-layer anisotropy models. Our new methodology is particularly helpful for temporary station deployments with limited recording times in order to utilize as many as possible signals including such with low-amplitude and small SNR.

**Key words:** Mantle processes; Body waves; Seismic anisotropy; Dynamics of lithosphere and mantle.

## 1 INTRODUCTION

Seismic anisotropy in the Earth's upper mantle is mainly caused by the preferred orientation of anisotropic minerals such as olivine (e.g. Nicolas & Christensen 1987; Ribe & Yu 1991). These phenomena provide an important proxy to describe the stress and strain regime of mantle dynamics driven by plate tectonic processes acting at depth (Savage 1999; Long & Becker 2010). The observation and analysis of birefringent teleseismic shear waves (SKS or SKKS) is frequently used to detect anisotropy deep inside the Earth (Vinnik *et al*. 1984; Kind *et al*. 1985; Silver & Chan 1988; Vinnik *et al*. 1989a). These waves propagate with a radial polarization after their conversion from a compressional wave to a shear wave at their exit from the core into the mantle. While propagating through anisotropic mantle material, the radially polarized shear wave splits into two orthogonally polarized shear waves that are identified by their elliptical polarization in the Radial-Transverse (R-T) plane. The delay time $\delta t$ between the split phases and the direction of fast wave polarization (given as angle $\Phi$ against north) are the so-called splitting parameters, which can be determined with several methods (Silver & Chan 1991; Long & van der Hilst 2005; Vecsey *et al*. 2008). However, a high signal-to-noise ratio (SNR), three or larger, is required on the T component (Vecsey *et al*. 2008) for a reliable determination of seismic anisotropy parameters.

The geodynamic interpretation of observed splitting is often limited to a simple, yet unrealistic, one-layer anisotropic model. The resolution of multiple-layer models requires observations from a wide backazimuth range. However, in many studies data from only a few backazimuth directions are available due to the heterogeneous distribution of hypocentres, low amplitude SKS signals and related low SNR. These problems arise especially for temporary station deployments with limited recording times and station sites with a low noise level.

[*] Now at: Berkeley Seismological Laboratory, UC Berkeley, Berkeley, CA, USA.
[†] Now at: Geosciences Department, Alfred Wegener Institute, Bremerhaven, Germany.
[‡] Also at: Department of Geosciences, CEED, University of Oslo, Oslo, Norway.

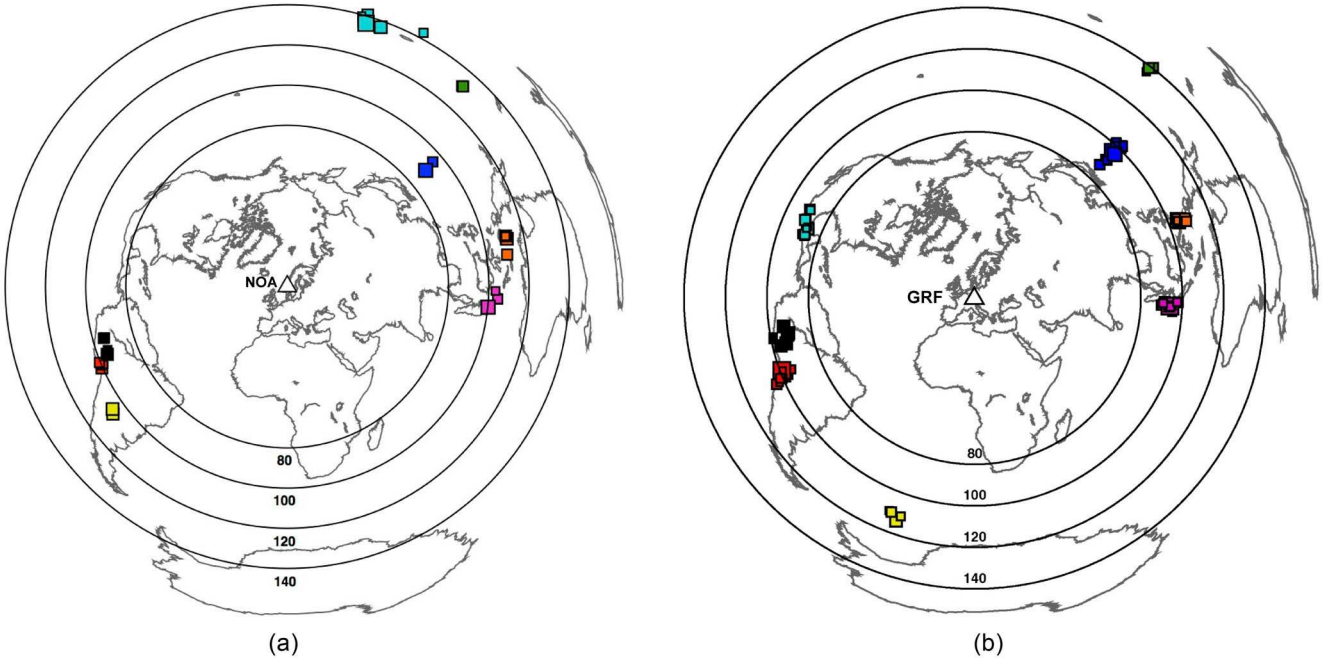


**Figure 1.** (a) Epicentre distribution with regional earthquake clusters below Fiji (6 events), Vanuatu (2), Mariana Islands (3), Banda Sea (4), Java (3), Southern Peru (5), Peru-Brasilia regions (4) and Santiago del Estero (2). The triangle indicates the centre of the large aperture NORSAR Array (NOA) and circles show distance in degree. (b) Epicentre distribution with regional earthquake clusters below Solomon Islands (3 events), Japan (18), Molucca Sea (16), Sumatra (16), South Sandwich Islands (8), Peru (10), Chile (15) and Mexico (14). The triangle indicates the Gräfenberg Array (GRF) and circles give distance in degree.

Typical SKS-source distributions are displayed in Fig. 1(a) for the years 1980–2011 as observed at the NORSAR Array (NOA) in Southern Norway and in Fig. 1(b) for the years 1976–2012 as observed at the Gräfenberg array (GRF) in Southern Germany. The displayed epicentres match the following selection criteria for SKS splitting analyses: distance range $85^\circ < \Delta < 140^\circ$, moment magnitude $6 < M_w < 7$ (NOA) and $5.5 < M_w < 7.5$ (GRF) and hypocentral depth $d > 100$ km (NOA) and $d > 25$ km (GRF). Mainly, earthquakes below South America and the Northwest Pacific region are useful, because the events from other regions provide only low-amplitude measurements with a too low SNR.

Here we introduce a method, which inverts $\delta t$ and $\Phi$ from multiple SKS recordings coincidently instead of single waveform inversions. We are able to determine stable splitting parameters even from low-amplitude observations. Better azimuthal coverage for future splitting analyses can be achieved with this method, and thus single- and multiple-layer anisotropic structures can be better resolved.

## 2 METHOD

### 2.1 Standard processing

Several methods exist to determine the splitting parameters $\delta t$ and $\Phi$ from split SKS phases, as reviewed by Long & van der Hilst (2005) and Vecsey *et al*. (2008). We apply the robust method of Silver & Chan (1991). The basic idea is to reverse the birefringent effect on the waveforms and find those $\delta t$ and $\Phi$ parameters for which the energy of the T component ($E_T$) is minimized. Using a grid search in the $\delta t$–$\Phi$ domain, the minimum $E_T$ is retrieved and confidence intervals for $\delta t$ and $\Phi$ are determined.

The R- and T-component waveforms, shown in Fig. 2(a), were processed in the following way: removal of a possible zero offset and trend in the originally recorded time-series, integration of the velocity-proportional broadband recordings to displacement, and frequency filtering (bandpass 0.067–0.2 Hz). The original north-south and east-west recorded components were rotated to R and T components based on the theoretical backazimuth to the source. Using a cosine-type time window, the SKS phase was extracted from the continuous time-series. The length of the time window depends on the individual SKS signal length.

Fig. 2 shows the T components of an earthquake under the Volcano Islands of 2007 September 28 recorded at seven NOA sites with clear SKS signals of about 20 per cent amplitude compared to the SKS phase on the R-component (see exemplary particle motion for site NC405 in Fig. 3c). We find a minimum at $\delta t \sim 0.6$ s and $\Phi \sim 146^\circ$ (indicated by the star in Fig. 3b) in the grid search at NC405. However, the uncertainty ranges of $\delta t$ and $\Phi$ are quite large, as shown by the broad 95 per cent confidence range in the $E_T^2$ contour plot, covering all possible values of $\Phi$ ($0^\circ$–$180^\circ$) for small $\delta t < 0.5$ s. It also contains another possible solution for $\Phi$ at around $40^\circ$ with an unresolved $\delta t$. This large uncertainty range is due to low SNR, the geometry of the measurement (angle between backazimuth and $\Phi$) as well as complex heterogeneous media with changing anisotropic properties, as known for Southern Norway and Sweden (Roy & Ritter 2013). The particle motion in the radial direction (Fig. 3d) is linear after correcting with the determined anisotropic parameters, as expected for an SKS wave in an isotropic medium. This successful correction in Fig. 3(d) is a strong argument that the determined anisotropy parameters are correct, however, it does not imply a unique solution (see large confidence interval in Fig. 3b).

### 2.2 Stacking techniques for SKS

Waveform stacking is a robust method to improve the SNR of low-amplitude seismic signals (e.g. Green *et al*. 1966). In such method,

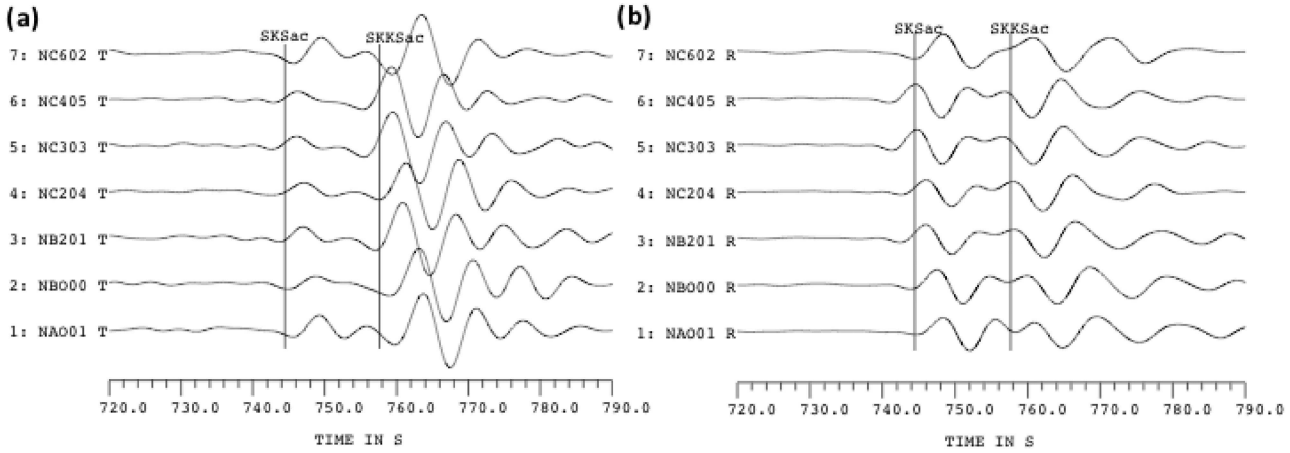


**Figure 2.** (a) Radial and (b) transverse component of SKS and SKKS waveforms of a Volcano Island earthquake (Mariana Trench) on 2007 September 28 recorded at the seven 3C NOA sites.

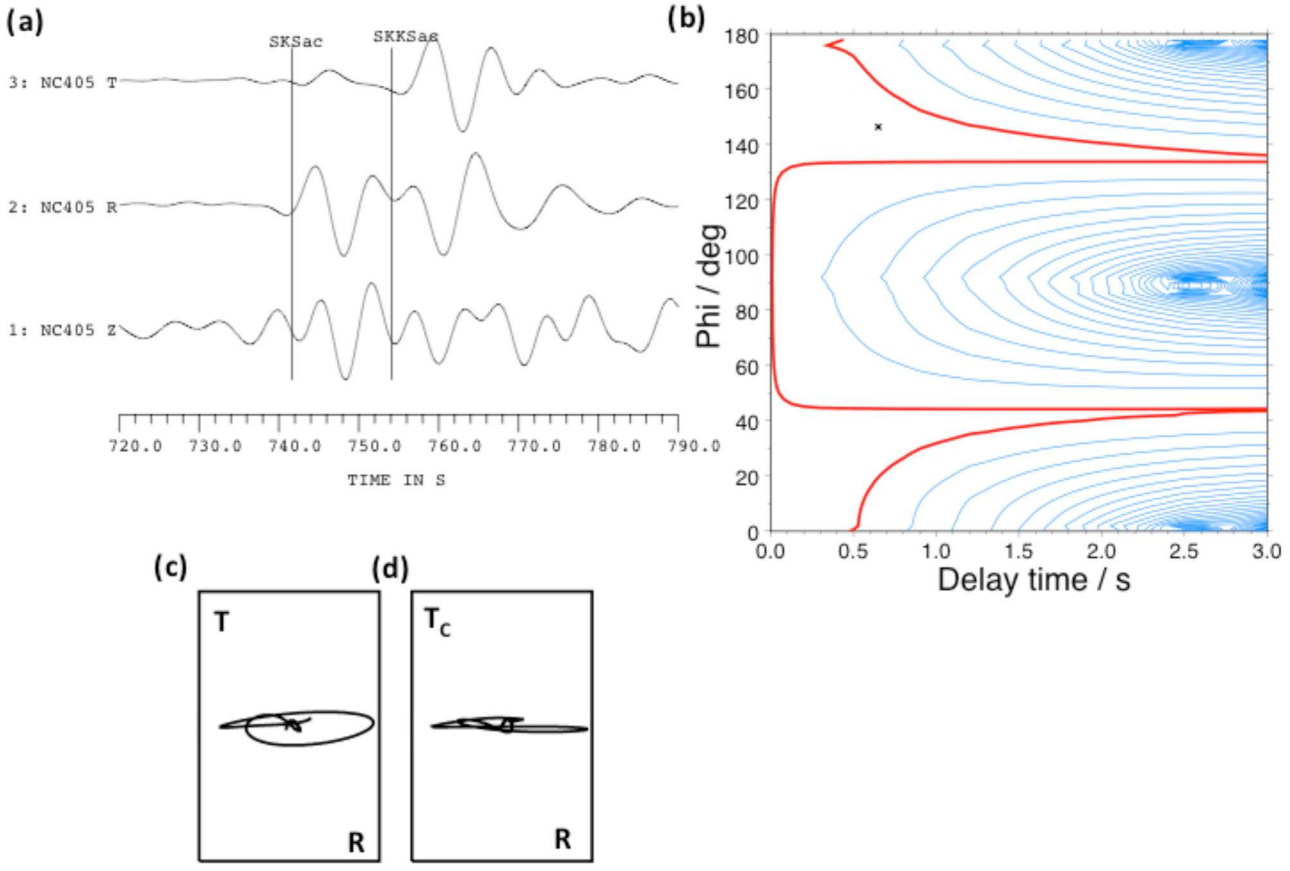


**Figure 3.** (a) SKS waveforms of a Volcano Island earthquake (Mariana Trench) on 2007 September 28 recorded at NOA site NC405. (b) Result of the splitting analysis as contours of the minimized energy on the transverse component ($E_T^2$), the red line displays the 95 per cent confidence region. (c) Measured particle motion. (d) Particle motion after correction for anisotropy with the splitting parameters $\Phi = 146^\circ$ and $\delta t = 0.7$ s (see star, panel b).

waveforms are aligned and stacked from the same seismic source recorded at different stations with incoherent background noise, including delay and sum, or slant stack. Rarely waveforms from different sources are stacked, for example, of repeating earthquakes (Yu & Wen 2012) or explosions (Krüger *et al*. 1993).

Gledhill & Gubbins (1996) stacked SKS waveforms of individual events at a nine-station network in New Zealand to perform a splitting analysis, which was otherwise not possible with single station recordings due to low SNR. As an alternative, Vinnik *et al*. (1989b) proposed the stacking of a residual function between observed and synthetic SKS waveforms. Wolfe & Silver (1998) stacked contour plots of the minimum eigenvalue of the corrected matrix of the particle motion. Roy & Ritter (2013) stacked SKS recordings at three neighbouring sites in a gliding window along a station profile in Norway and Sweden to stabilize the splitting analysis. Such an approach is only valid, if the anisotropic structure underneath the different stations is nearly identical and a common Fresnel zone is covered by only slightly different recording geometries. Otherwise,

the split SKS waveforms would differ at the various stations and the stacking procedure would distort the result, because the splitting information in the waveform is not stacked constructively.

### 2.3 Simultaneous Inversion of Multiple Waveforms (SIMW)

Here we introduce a new method of stacking SKS and SKKS waveforms. The aim is to improve the SNR to allow a more stable splitting analysis for seismic source regions, from which only low-SNR recordings are available. The main idea is to invert several SKS/SKKS waveforms simultaneously for a common splitting parameter set ($\delta t$ and $\Phi$) by concatenating the waveforms. In this way a new waveform, composed of several SKS/SKKS phases, is generated and used to determine $\delta t$ and $\Phi$ instead of using a single SKS/SKKS recording. As for classical seismic beam forming techniques (for an overview, see Schweitzer *et al*. 2012) we make the assumption that the noise energy during the different SKS/SKKS time windows is different and incoherent, while the SKS/SKKS splitting function is identical for all SKS/SKKS observations. The goal is to find a combination of common splitting parameters, which best reduces the energy on the T component for all SKS/SKKS observations. One can concatenate recorded SKS/SKKS phases from one earthquake recorded at different stations (*station stack*) and/or concatenate recordings from different events from the same source region measured at a single seismic station (*source stack*).

The specific data processing for SIMW involves the extraction of time windows of similar length with different SKS/SKKS phases on the T and R component and tapering with a cosine window to prevent undesired steps in the time-series.

Next, the waveforms of both components are normalized relative to the R component. This normalization mitigates amplitude variations due to magnitude variations of the source and prevents the final result from being dominated by one specific recording with large amplitude. Optionally, a frequency bandpass filter can be applied and then the single waveforms are concatenated to one long time-series. Finally, we perform an inversion of the complete waveform using the method of Silver & Chan (1991). Other inversion procedures (Long & van der Hilst 2005 or Vecsey *et al*. 2008) may work, but have not yet been tested. Inversions were performed using SplitLab (Wüstefeld *et al*. 2008) for the GRF waveforms and a standard Silver & Chan inversion code for the NOA waveforms. The potential of the SIMW method is demonstrated in the following three examples.

In Fig. 4(a), we show the concatenated SKS waveforms from one earthquake underneath the Volcano Islands (Mariana Trench) on

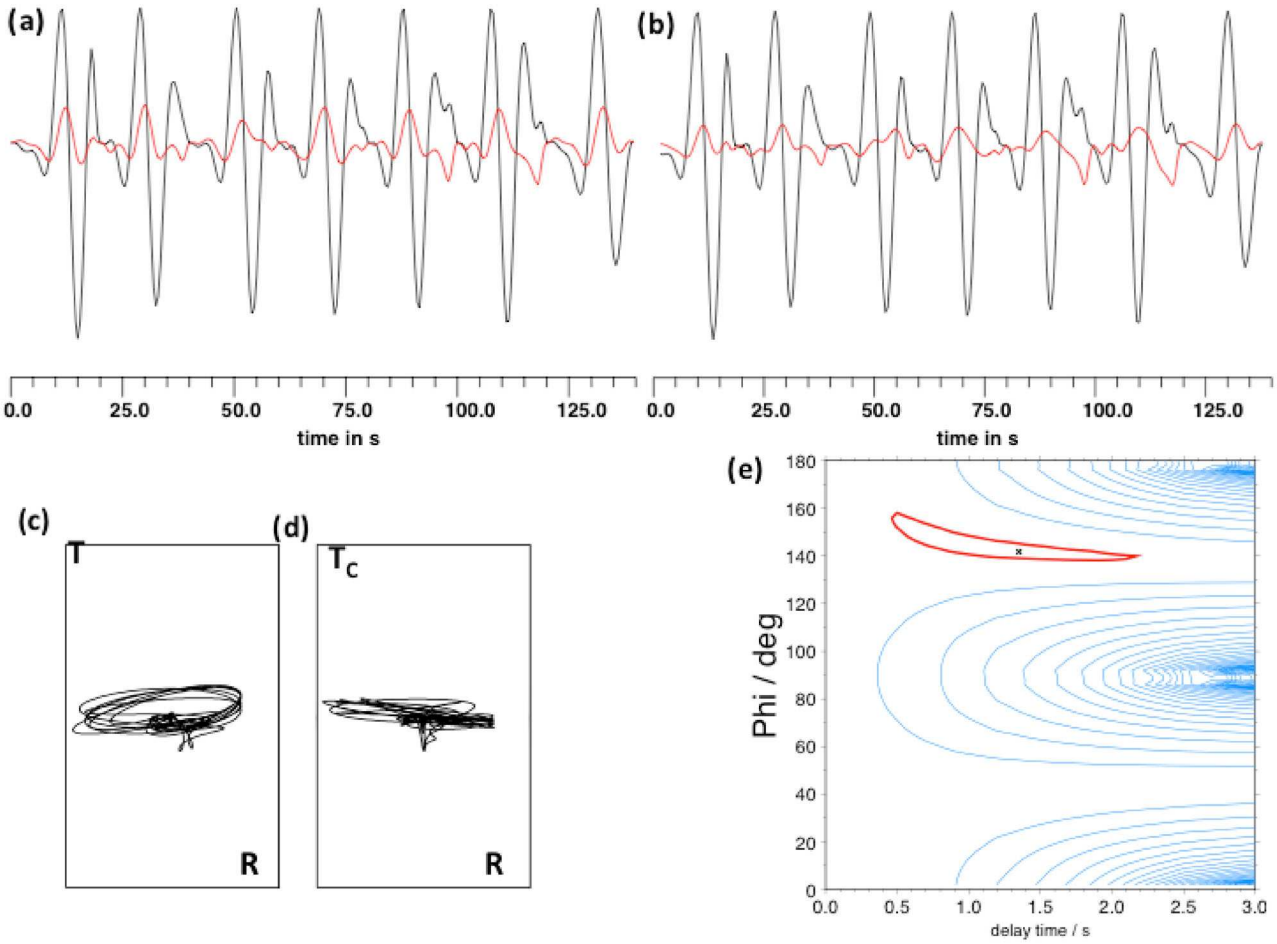


**Figure 4.** Station stack: simultaneous inversion of seven SKS phases from one Mariana Island earthquake (2007 September 28) recorded at the seven NOA sites (see Fig. 2). (a) Concatenated waveforms (red: transverse, black: radial) after normalization with the SKS phase on the radial component. (b) Concatenated waveforms (red: transverse, black: radial) after correction with the splitting parameters $\Phi = 142^\circ$ and $\delta t = 1.4$ s. (c,d) Particle motion of the waveforms before and after correction of anisotropy. (e) Result of the splitting analysis as contours of the minimized energy of the transverse component ($E_T^2$) of the concatenated waveforms, the red line displays the 95 per cent confidence region.

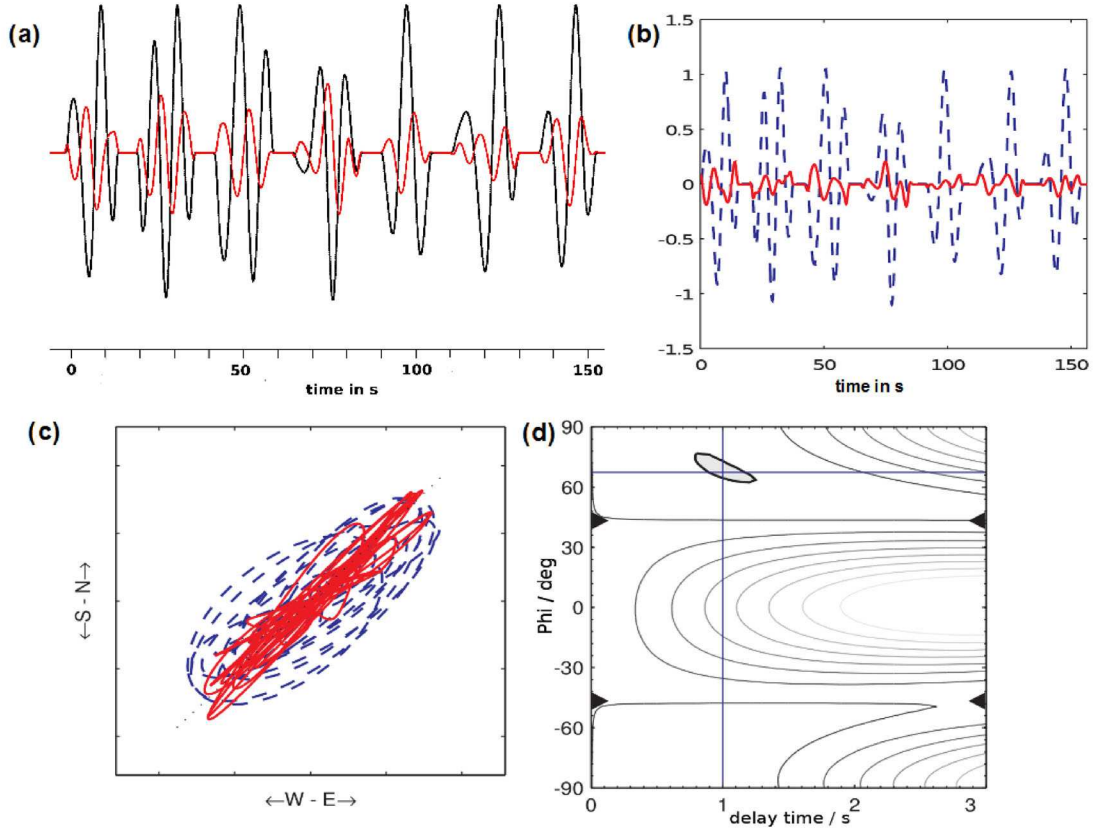


**Figure 5.** Simultaneous inversion of seven SKS phases from seven different earthquakes near Japan recorded at Gräfenberg station GRA1. (a) Concatenated waveforms (black: radial, red: transverse) after normalization of the radial component per SKS phase. (b) Concatenated waveforms (blue: radial, red: traverse) after correction with the splitting parameters $\Phi = 67^\circ$ and $\delta t = 1.0$ s. (c) Particle motion of the measured waveforms (blue: normalized concatenated waveform) and of the corrected concatenated waveform (red). (d) Result of the splitting analysis as contours of the minimized energy ($E_T^2$) for the waveform in (a). The 95 per cent confidence level is given in grey.

2007 September 28 recorded at the seven NOA sites (station stack) as shown in Fig. 2. The elliptical polarization (Fig. 4c) indicates SKS splitting, although the SNR is smaller than 3 on the T component.

The minimum $E_T^2$ located within the grid search of concatenated SKS waveforms (Fig. 4e) is clearly better confined than the inversion of the single waveform in Fig. 3(b). The particle motion of the corrected concatenated waveforms (Fig. 4d) is linear in radial direction for all seven corrected SKS waveforms, indicating a successful correction for anisotropy with the determined splitting parameters. The concatenated corrected waveforms (Fig. 4b) show a clear reduction of the amplitude during the arrival time of the SKS phase on the transverse component.

In Fig. 5(a), we show the concatenated SKS waveforms from seven different earthquakes beneath Japan recorded at station GRA1 of the Gräfenberg array (source stack). The minimum of $E_T^2$ is clearly defined within a very small 95 per cent confidence region (Fig. 5d) and the particle motion (Fig. 5c) is almost linear after the correction for anisotropy. This example demonstrates that the splitting parameters, obtained by minimizing $E_T^2$ for several waveforms coincidently, can explain the recorded data very well.

In Fig. 6(a), we compare the single splitting measurements for three earthquakes under the Mariana Islands region with the SIMW results at 3 NOA sites (Table 1). The 95 per cent confidence interval for the SIMW results at the NOA sites NA001 and NC602 are clearly reduced compared to the single splitting measurements, demonstrating the improvement in the determination of the splitting parameters. The SIMW result for site NC405 is similar to the single event on 1996 June 9 but better constrained compared to the single event results on 2001 July 3 and 2007 September 28. Moreover, a narrow confidence range confines the $\delta$t value when applying SIMW. In Fig. 6(b), we show the comparison of single splitting measurements with the SIMW result at GRB1 station for three earthquakes beneath Chile and Japan. Again, the confidence intervals are clearly reduced in both examples for the SIMW result. For the Chile earthquake the uncertainties in $\delta$t are considerably reduced by the SIMW method, even if the confidence regions of the single splitting measurements are already quite confined. In the Japan example in Fig. 6(b), especially the result for the fast axis $\Phi$ is improved by the SIMW method.

In the following we present more details on the resolution power of SIMW for the NOA and GRF recordings.

## 3 SIMW RESULTS FOR NOA

Applying the SIMW algorithm at NOA stations, waveforms from eight different source regions are used for a SKS / SKKS splitting analysis (Fig. 1a) with seismic events of similar backazimuth ($\pm 2^\circ$). In increasing backazimuth order, these source regions are: Fiji Islands, Vanuatu, Mariana Islands, Banda Sea, Java, Southern Peru, Peru-Brazil border and Santiago/Chile (Table 1). This source distribution for SIMW contains two additional backazimuth directions compared to the earlier work of Roy & Ritter (2013). Additionally, more stable splitting results were determined at six out of seven NOA sites, where none were available before. For the Fiji Islands

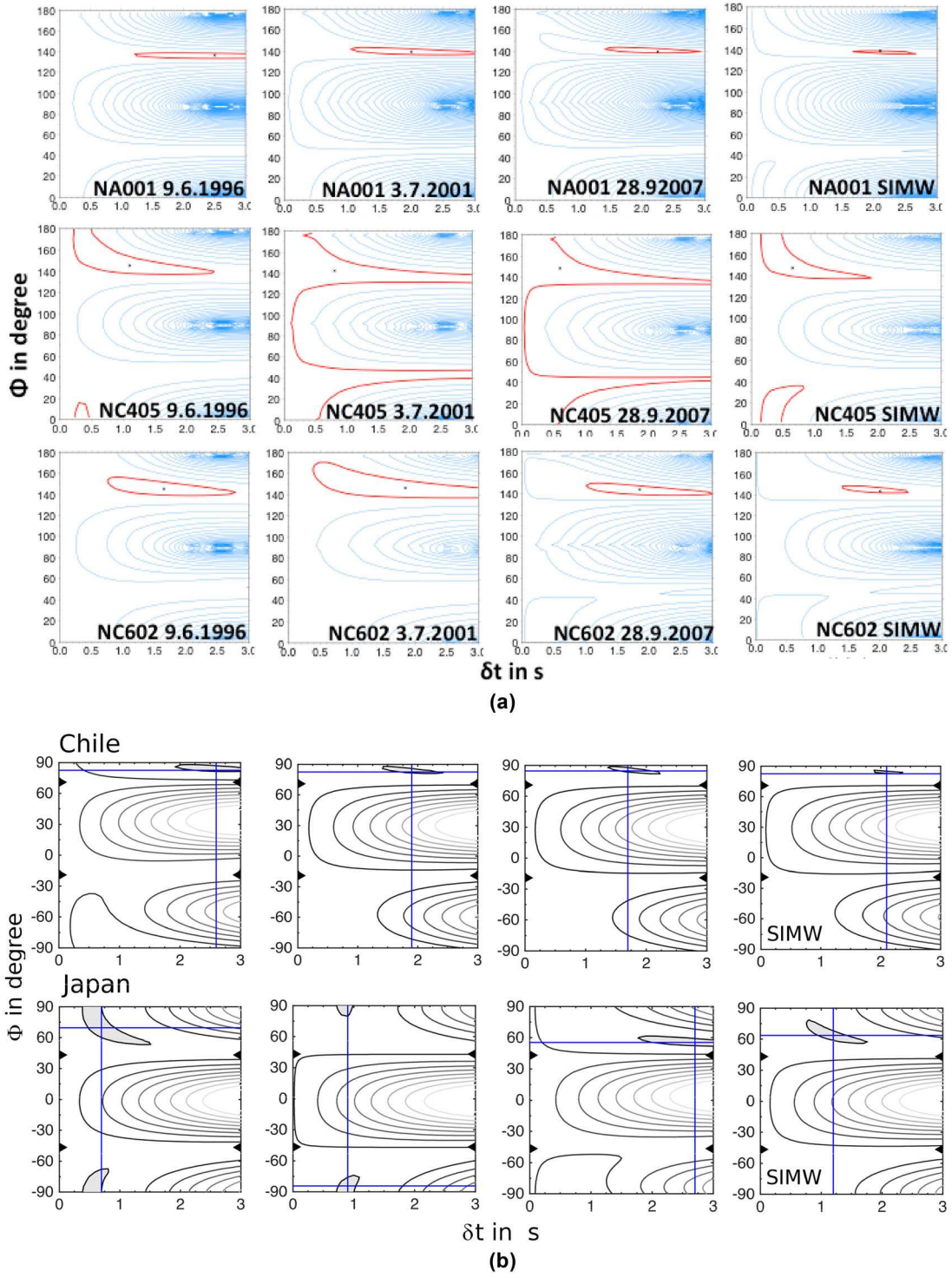


**Figure 6.** (a) Comparison of single splitting measurements with the results of a simultaneous inversion of SKS phases of different events (SIMW) at the NOA sites NA001, NC405 and NC602 (right column). All events occurred beneath the Mariana Islands region (Table 1). Contours indicate the minimized energy of the transverse component ($E_T^2$) of the waveforms, the red line displays the 95 per cent confidence region. (b) Comparison of single splitting measurements recorded at the station GRB1 with the SIMW results (right column). Events occurred beneath Chile and Japan. The grey area gives the 95 per cent confidence region.

region, SKS phases of seven events could be analysed, however, not all of these were recorded at all 3C NOA site due to too low SNR or station outages.

The splitting parameters from the previous study (Roy & Ritter 2013) and the SIMW method are compared in Fig. 7. The arrows indicate the fast wave polarization direction, their length corresponds to the delay time and the colour indicates the source region following the colouring in Fig. 1(a). SIMW results at sites NC303, NC405 and NC602 reveal a clear backazimuth dependence of the splitting parameters (Fig. 7b), which was not observed previously (Fig. 7a).

**Table 1.** Splitting measurements per event and station listed for different source regions. The analysed phase (SKS or SKKS) is given below the event time. SIMW is the result of the simultaneous inversion of multiple waveforms for all SKS or SKKS recordings of a source region. Errors fnond to the 95 per cent confidence interval as determined by the $E_T^2$ minimization (see the text). Empty cells indicate events where the splitting parameters could not be determined due to a low SNR or a non-linear particle motion after the correction.

| Fiji Islands | | | | BAZ∼14° | | | | |
|---|---|---|---|---|---|---|---|---|
| | NAO01 | NB201 | NBO00 | NC204 | NC303 | NC405 | NC602 | |
| 09.06.1991 | – | – | – | 40° ± 30° | 19° ± 25 | No data | 23° ± 2° | Φ |
| SKKS | | | | 1.4 ± 1.3 | 3 ± 2.3 | | 3 ± 0.4 | $\delta t$ / s |
| 16.04.1993 | – | No data | – | – | 8° ± 10° | No data | 18° ± 45° | Φ |
| SKS | | | | | 2.4 ± 0.8 | | 2.9 ± 1.5 | $\delta t$ / s |
| 29.03.1998 | – | – | 107° ± 45° | – | 110° ± 45° | No data | – | Φ |
| SKS | | | 2.4 ± 1.5 | | 3 ± 1.0 | | | $\delta t$ / s |
| 28.04.2001 | 21° ± 45° | – | 1° ± 45° | – | 21° ± 45° | – | No data | Φ |
| SKS | 3 ± 0.8 | | 3 ± 1.5 | | 3 ± 1.5 | | | $\delta t$ / s |
| 19.08.2002 | 35° ± 45° | 53° ± 30° | 28° ± 15° | – | – | 22° ± 45° | 30° ± 3° | Φ |
| SKKS | 0.8 ± 0.8 | 0.7 ± 0.7 | 1.9 ± 0.8 | | | 2.5 ± 1.5 | 2.4 ± 0.6 | $\delta t$ / s |
| 19.07.2008 | – | – | 35° ± 45° | – | – | – | – | Φ |
| SKS | | | 1.9 ± 0.8 | | | | | $\delta t$ / s |
| SIMW | 29° ± 30 | – | 69° ± 30° | – | 30° ± 45° | – | – | Φ |
| SKS | 1 ± 1.2 | | 1.2 ± 0.8 | | 1.2 ± 1.5 | | | $\delta t$ / s |
| SIMW | – | – | – | – | – | – | 23° ± 3° | Φ |
| SKKS | | | | | | | 2.9 ± 0.7 | $\delta t$ / s |
| Vanuatu | | | | BAZ∼31° | | | | |
| | NAO01 | NB201 | NBO00 | NC204 | NC303 | NC405 | NC602 | |
| 17.03.1996 | – | 41° ± 45° | – | – | – | – | 37° ± 45° | Φ |
| SKS | | 3 ± 0.8 | | | | | 3 ± 0.8 | $\delta t$ / s |
| 17.03.1996 | 139° ± 45° | – | 140° ± 25° | – | – | 130° ± 45° | 137° ± 45° | Φ |
| SKKS | 1.4 ± 1.5 | | 1.3 ± 1 | | | 1.8 ± 1.5 | 2.9 ± 0.8 | $\delta t$ / s |
| 10.08.1988 | 63° ± 45° | 41° ± 14° | No data | – | 47° ± 45° | No data | 52° ± 45° | Φ |
| SKS | 1.5 ± 0.8 | 3 ± 0.8 | | | 2.2 ± 0.8 | | 1.7 ± 0.8 | $\delta t$ / s |
| 10.08.1988 | 9° ± 45° | – | No data | – | 41° ± 45° | No data | – | Φ |
| SKKS | 1.9 ± 0.8 | | | | 3 ± 0.8 | | | $\delta t$ / s |
| SIMW | – | 41° ± 1.5° | – | – | – | – | 40° ± 14° | Φ |
| SKS | | 3 ± 0.1 | | | | | 3 ± 0.7 | $\delta t$ / s |
| SIMW | 155° ± 45° | – | – | – | – | – | – | Φ |
| SKKS | 1 ± 0.8 | | | | | | | $\delta t$ / s |
| Mariana Islands | | | | BAZ∼40° | | | | |
| | NAO01 | NB201 | NBO00 | NC204 | NC303 | NC405 | NC602 | |
| 09.06.1996 | 141° ± 5° | – | – | – | – | 145° ± 20° | 145° ± 10° | Φ |
| SKS | 2.5 ± 1 | | | | | 1.1 ± 1.5 | 1.7 ± 1 | $\delta t$ / s |
| 03.07.2001 | 140° ± 5° | 144° ± 10° | 140° ± 44° | 142° ± 45° | 148° ± 10° | 142° ± 45° | 146° ± 20° | Φ |
| SKS | 2.1 ± 1 | 1.6 ± 1.1 | 1.4 ± 1.6 | 1.5 ± 1.5 | 1.1 ± 0.1 | 0.7 ± 2.3 | 1.9 ± 1.3 | $\delta t$ / s |
| 28.09.2007 | 140° ± 2° | 142° ± 10° | 138° ± 5° | 142° ± 45° | 148° ± 5° | 148° ± 45° | 144° ± 10° | Φ |
| SKS | 2.3 ± 0.7 | 1.8 ± 1.2 | 1.8 ± 1 | 1.6 ± 1.4 | 1.1 ± 0.5 | 0.6 ± 2.3 | 1.9 ± 1 | $\delta t$ / s |
| SIMW | 139° ± 0.6 | 142° ± 5° | 138° ± 10° | 144° ± 20° | 148° ± 20° | 147° ± 20° | 143° ± 2° | Φ |
| SKS | 2.1 ± 0.2 | 1.8 ± 0.6 | 1.5 ± 0.6 | 1.3 ± 0.7 | 1 ± 0.7 | 0.7 ± 0.5 | 2 ± 0.3 | $\delta t$ / s |
| Banda Sea | | | | BAZ∼66° | | | | |
| | NAO01 | NB201 | NBO00 | NC204 | NC303 | NC405 | NC602 | |
| 07.10.1982 | – | – | – | 139° ± 35° | 156° ± 5° | 152° ± 5° | – | Φ |
| SKS | | | | 2.3 ± 0.7 | 3 ± 1.8 | 3 ± 1.1 | | $\delta t$ / s |
| 07.10.1982 | 75° ± 45° | – | – | 141° ± 45° | – | – | – | Φ |
| SKKS | 2.8 ± 0.8 | | | 1.3 ± 0.7 | | | | $\delta t$ / s |
| 02.03.2005 | – | – | – | – | 146° ± 45° | 138° ± 13° | – | Φ |
| SKS | | | | | 1.5 ± 1.5 | 1.3 ± 1 | | $\delta t$ / s |
| 02.03.2005 | – | – | – | – | – | – | – | Φ |
| SKKS | | | | | | | | $\delta t$ / s |
| 04.08.2008 | 239° ± 45° | – | – | – | – | – | – | Φ |
| SKS | 2.1 ± 0.9 | | | | | | | $\delta t$ / s |
| 24.10.09 | – | – | 148° ± 3° | 144° ± 17° | 145° ± 43° | 149° ± 5° | – | Φ |
| SKS | | | 2.3 ± 0.3 | 1.9 ± 1.2 | 1.7 ± 1.7 | 2.4 ± 1 | | $\delta t$ / s |
| 24.10.09 | – | – | – | 126° ± 45° | – | – | – | Φ |
| SKKS | | | | 0.6 ± 1.5 | | | | $\delta t$ / s |

**Table 1** (*Continued.*)

| Banda Sea | | | | BAZ∼66° | | | | |
|---|---|---|---|---|---|---|---|---|
| | NAO01 | NB201 | NBO00 | NC204 | NC303 | NC405 | NC602 | |
| SIMW | – | – | – | 147° ± 15° | 152° ± 6° | 150° ± 3° | – | Φ |
| SKS | | | | 1.4 ± 0.8 | 1.7 ± 0.6 | 1.7 ± 0.8 | | $\delta t$ / s |
| SIMW | – | – | – | 117° ± 45° | – | – | – | Φ |
| SKKS | | | | 0.6 ± 1.3 | | | | $\delta t$ / s |
| Java | | | | BAZ∼82° | | | | |
| | NAO01 | NB201 | NBO00 | NC204 | NC303 | NC405 | NC602 | |
| 28.09.1998 | 90° ± 10° | 106° ± 25° | 148° ± 25° | 124° ± 26° | 122° ± 15° | no | 117° ± 30° | Φ |
| SKS | 1.7 ± 1.3 | 1.0 ± 0.8 | 0.8 ± 0.7 | 0.7 ± 0.4 | 0.8 ± 0.2 | | 0.3 ± 0.4 | $\delta t$ / s |
| 08.08.1985 | – | 164° ± 2° | 92° ± 34° | No data | No data | No data | 89° ± 1° | Φ |
| SKS | | 3 ± 1.3 | 1 ± 1.3 | | | | 3 ± 0.8 | $\delta t$ / s |
| 08.08.2007 | – | 130° ± 45° | 103° ± 15° | 115° ± 45° | – | – | – | Φ |
| SKS | | 0.7 ± 1.5 | 1 ± 0.6 | 0.6 ± 1.5 | | | | $\delta t$ / s |
| SIMW | – | 140° ± 30° | 114° ± 23° | 132° ± 25° | – | – | 87° ± 2° | Φ |
| SKS | | 0.7 ± 0.6 | 0.6 ± 0.2 | 0.6 ± 0.4 | | | 3 ± 2.0 | $\delta t$ / s |
| Southern Peru | | | | BAZ∼250° | | | | |
| | NAO01 | NB201 | NBO00 | NC204 | NC303 | NC405 | NC602 | |
| 18.06.1984 | – | No data | 154° ± 33° | 90° ± 17° | No data | No data | No data | Φ |
| SKS | | | 1.1 ± 1.1 | 1.3 ± 0.8 | | | | $\delta t$ / s |
| 24.05.1991 | 175° ± 30° | – | 81° ± 7° | 82° ± 2° | 87° ± 16° | 81° ± 1° | 173° ± 5° | Φ |
| SKS | 1.0 ± 0.6 | | 1.5 ± 0.6 | 2.7 ± 0.8 | 1 ± 1.2 | 3 ± 0.8 | 3 ± 1.5 | $\delta t$ / s |
| 08.10.1998 | – | – | 83° ± 45° | 85° ± 5° | 111° ± 30° | No data | 20° ± 19° | Φ |
| SKS | | | 2.4 ± 0.8 | 3 ± 1 | 0.9 ± 1.0 | | 0.9 ± 0.6 | $\delta t$ / s |
| 04.07.2008 | – | – | 82° ± 45° | – | 88° ± 13° | – | 0° ± 45° | Φ |
| SKS | | | 2.8 ± 0.8 | | 1.4 ± 1.8 | | 1.7 ± 1.3 | $\delta t$ / s |
| 12.07.2009 | – | 83° ± 45° | 83° ± 45° | 85° ± 2° | 86° ± 45° | 88° ± 45° | 6° ± 25° | Φ |
| SKS | | 1.6 ± 1.5 | 2.9 ± 1.5 | 2.6 ± 0.3 | 1.8 ± 0.8 | 1.0 ± 1.5 | 1.3 ± 0.8 | $\delta t$ / s |
| SIMW | – | – | 82° ± 1° | 84° ± 1° | 83° ± 15° | 81° ± 2° | 180° ± 5° | Φ |
| SKS | | | 2.4 ± 0.4 | 2.7 ± 0.4 | 1.0 ± 0.6 | 2.6 ± 1 | 1.6 ± 0.7 | $\delta t$ / s |
| Peru-Brazil border region | | | | BAZ∼260° | | | | |
| | NAO01 | NB201 | NBO00 | NC204 | NC303 | NC405 | NC602 | |
| 02.06.1983 | 74° ± 45° | No data | – | 114° ± 22° | – | – | 173° ± 1° | Φ |
| SKS | 3 ± 1.5 | | | 1.2 ± 0.6 | | | 3 ± 1.3 | $\delta t$ / s |
| 03.12.1989 | – | – | – | – | – | – | 91° ± 6° | Φ |
| SKS | | | | | | | 3 ± 1.9 | $\delta t$ / s |
| 17.10.1990 | – | – | 161° ± 45° | – | 95° ± 30° | 86° ± 12° | 176° ± 4° | Φ |
| SKS | | | 1.3 ± 1.5 | | 1.3 ± 0.8 | 1.6 ± 1.3 | 3 ± 1.5 | $\delta t$ / s |
| 03.04.1998 | – | – | – | – | 151° ± 45° | – | 5° ± 45° | Φ |
| SKS | | | | | 1.5 ± 0.8 | | 3 ± 0.8 | $\delta t$ / s |
| SIMW | – | – | – | – | 142° ± 35° | – | 175° ± 5° | Φ |
| | | | | | 1.1 ± 1.4 | | 3 ± 0.7 | $\delta t$ / s |
| Santiago del Estero | | | | BAZ∼242° | | | | |
| | NAO01 | NB201 | NBO00 | NC204 | NC303 | NC405 | NC602 | |
| 23.06.1991 | 159° ± 4° | No data | – | 69° ± 2° | – | – | – | Φ |
| SKS | 3 ± 1.5 | | | 3 ± 0.8 | | | | $\delta t$ / s |
| 23.04.2000 | – | – | – | 70° ± 1° | – | No data | 162° ± 45° | Φ |
| SKS | | | | 3 ± 0.9 | | | 1.5 ± 1.5 | $\delta t$ / s |
| SIMW | – | – | – | 69° ± 1° | – | – | – | Φ |
| SKS | | | | 3 ± 0.5 | | | | $\delta t$ / s |

Contrariwise the results at sites NBO00 and NC204 only indicate that the fast polarization direction is different for opposing backazimuths, namely east-west for arrivals from Peru and north-east for arrivals from the Mariana Island region.

At site NB201 no backazimuth dependence of the splitting parameters is observed (Fig. 7). The fast polarization axis for SKS phases arriving from Peru (red) coincides at all NOA sites, except for station NC602. Partly, the fast polarization axes do not vary much between the NOA sites for the same backazimuth directions, suggesting that the mantle structure beneath the sites may be similar. The fast axes at all sites have in general small error bars especially at site NC602 (<5°) (Fig. 8) and are, therefore, considered reliable. The delay times $\delta t$ are as large as 3 s, again preferentially at station NC602. This large value may be due to the thick lithosphere compared to smaller $\delta t$ values in Central Europe (see GRF results below) as well as a local splitting anomaly. The dependency on the backazimuth leads to the conclusion that a more complex structure than a single anisotropic layer is needed to explain the splitting

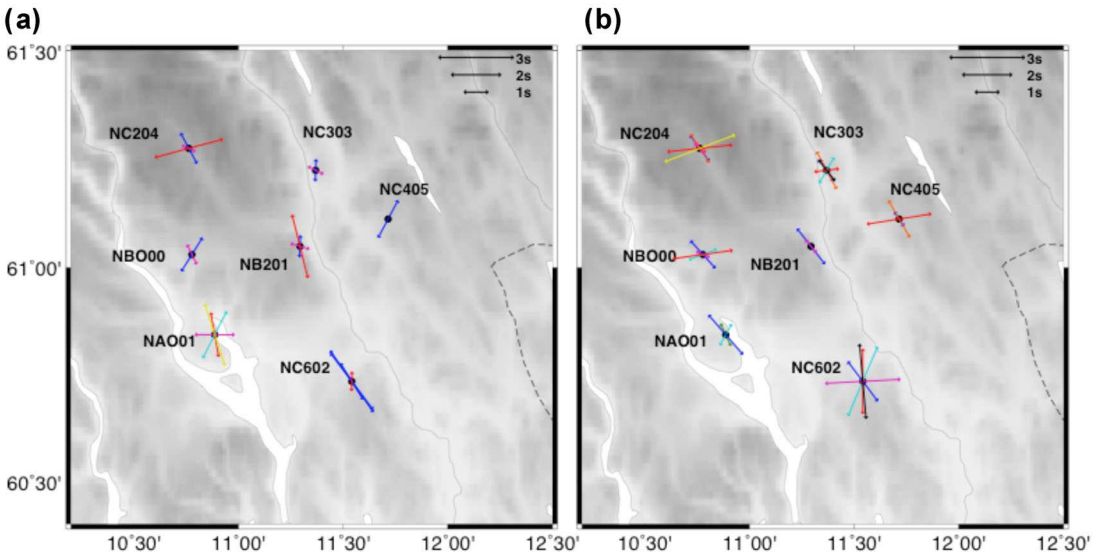


**Figure 7.** Splitting results at the 3C sites of the NOA Array in Southern Norway. Arrow direction is in direction of fast shear wave polarization, arrow length is proportional to delay time and the colour corresponds to the source region (see Fig. 1a). (a) Previous results from Roy & Ritter (2013) using single SKS recordings at each station. (b) New results obtained from the simultaneous inversion of multiple waveforms (SIMW).

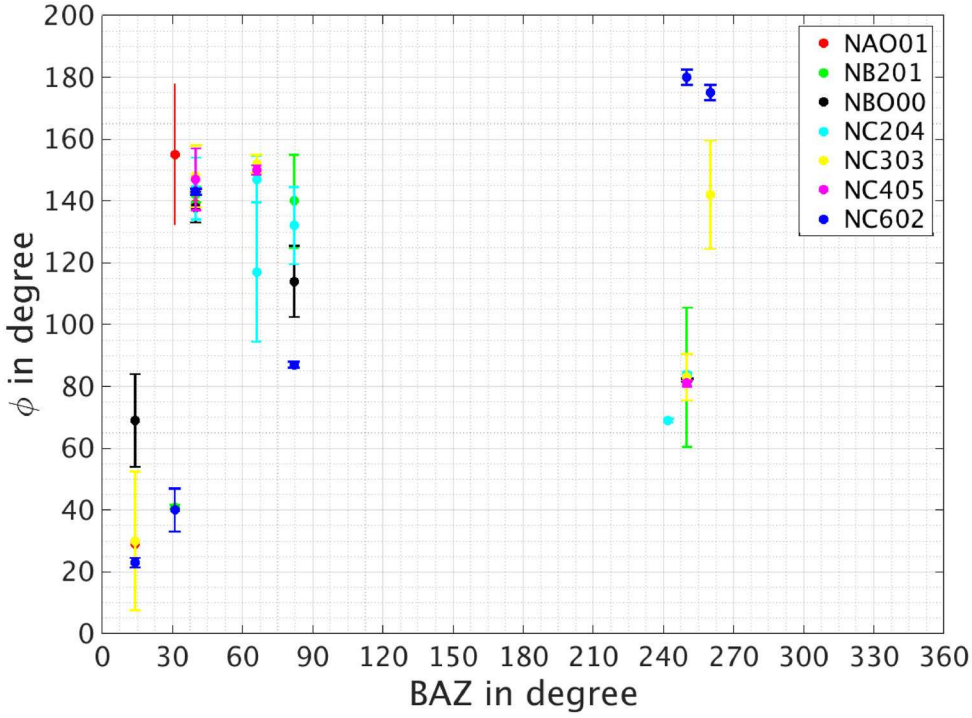


**Figure 8.** Fast polarization direction Φ and errors as function of backazimuth for the SIMW method at the NOA sites.

results at NOA. This will be analysed in more details in a separate study.

## 4 SIMW RESULTS FOR GRF

The splitting parameters Φ and $\delta t$ were determined with the SIMW method for the three stations GRA1, GRB1, GRC1 of the Gräfenberg array (GRF), which had three component recordings since the beginning of the observational period (Harjes & Seidl 1978). Previous studies resulted in diverse models for anisotropy (Table 3) and indicate a complex tectonic situation due to the transition between two Variscan terranes. Earthquakes with SKS phases suitable for this study were recorded from eight source regions (Fig. 1b). The results for Φ and $\delta t$ are listed in Table 2. As an example, all results based on the standard single waveform analysis and the SIMW method are listed for the Molucca Sea source region. All SIMW results for the three GRF stations are shown in Figs 9 and 10, colours indicate the source regions, corresponding to Fig. 1(b).

At stations GRB1 and GRC1, Φ is orientated predominantly east-west with only two and one exceptions, respectively. On the contrary, the Φ directions at station GRA1 vary with backazimuth. The delay times obtained with SIMW are mostly between 1 and

**Table 2.** Splitting measurements per event and station of the Gräfenberg Array listed for different source regions. SIMW is the simultaneous inversion waveform results for all single events of a source region. The number and type of simultaneously analysed phases per station is given in the left column. Errors correspond to the 95 per cent confidence interval as determined from the $E_T$ minimization.

| Molucca Sea | | BAZ ~ 69° | | |
|---|---|---|---|---|
| | GRA1 | GRB1 | GRC1 | |
| 26/10/84 | 78° ± 4° | | | Φ |
| SKS | 3.0 ± 0.4 | | | $\delta t$ / s |
| 21/01/85 | | | 117° ± 19° | Φ |
| SKS | | | 0.8 ± 0.2 | $\delta t$ / s |
| 12/07/86 | | | 135° ± 27° | Φ |
| SKS | | | 0.9 ± 0.7 | $\delta t$ / s |
| 14/08/86 | 78° ± 5° | 79° ± 5° | | Φ |
| SKS | 3.0 ± 0.7 | 3.0 ± 1.0 | | $\delta t$ / s |
| 15/08/86 | | 81° ± 5° | 143° ± 9° | Φ |
| SKS | | 1.7 ± 0.8 | 1.2 ± 0.5 | $\delta t$ / s |
| 16/08/86 | | 81° ± 8° | | Φ |
| SKS | | 1.9 ± 1.0 | | $\delta t$ / s |
| 07/11/88 | | 89° ± 13° | 91° ± 25° | Φ |
| SKS | | 0.6 ± 0.3 | 0.8 ± 0.4 | $\delta t$ / s |
| 14/09/89 | 74° ± 3° | 89° ± 26° | 137° ± 13° | Φ |
| SKS | 3.0 ± 0.5 | 0.6 ± 0.5 | 0.8 ± 0.3 | $\delta t$ / s |
| 30/05/93 | | 77° ± 41° | 77° ± 7° | Φ |
| SKS | | 1.1 ± 1.4 | 1.2 ± 0.7 | $\delta t$ / s |
| 28/02/96 | 76° ± 22° | 131° ± 36° | | Φ |
| SKS | 1.6 ± 1.5 | 0.4 ± 0.6 | | $\delta t$ / s |
| 17/09/97 | | | 101° ± 37° | Φ |
| SKS | | | 0.6 ± 0.9 | $\delta t$ / s |
| 26/09/00 | 86° ± 11° | | 91° ± 35° | Φ |
| SKS | 1.6 ± 1.5 | | 0.8 ± 1.0 | $\delta t$ / s |
| 24/02/01 | | | 77° ± 3° | Φ |
| SKS | | | 2.2 ± 0.8 | $\delta t$ / s |
| 04/08/01 | | | 87° ± 5° | Φ |
| SKS | | | 1.5 ± 0.6 | $\delta t$ / s |
| 27/08/01 | 82° ± 3° | | | Φ |
| SKS | 1.9 ± 0.4 | | | $\delta t$ / s |
| 14/03/10 | | | 95° ± 25° | Φ |
| SKS | | | 1.4 ± 0.7 | $\delta t$ / s |
| 26/08/12 | 88° ± 25° | 103° ± 17° | 105° ± 30° | Φ |
| SKS | 0.4 ± 0.7 | 0.4 ± 0.2 | 0.3 ± 0.3 | $\delta t$ / s |
| SIMW | 76° ± 2° | 81° ± 5° | 97° ± 8° | Φ |
| 7 SKS, 8 SKS, 12 SKS | 2.9 ± 0.6 | 1.2 ± 0.4 | 0.7 ± 0.2 | $\delta t$ / s |
| Japan | | BAZ ~ 43° | | |
| SIMW | 77° ± 5° | 88° ± 7° | 85° ± 3° | Φ |
| 18 SKS, 11 SKS, 11 SKS | 0.9 ± 0.1 | 0.8 ± 0.1 | 1.3 ± 0.1 | $\delta t$ / s |
| Sumatra | | BAZ ~ 91° | | |
| SIMW | 7° ± 4° | 91° ± 3° | 63° ± 25° | Φ |
| 4 SKS, 10 SKS, 9 SKS | 2.0 ± 0.8 | 3.0 ± 0.8 | 0.6 ± 0.4 | $\delta t$ / s |
| South Sandwich Islands | | BAZ ~ 199° | | |
| SIMW | 29° ± 16° | 68° ± 9° | 76° ± 6° | Φ |
| 8 SKS, 3 SKKS, 1 SKKS | 1.8 ± 1.2 | 1.2 ± 0.2 | 1.3 ± 0.2 | $\delta t$ / s |
| Chile | | BAZ ~ 248° | | |
| SIMW | 80° ± 1° | 85° ± 1° | 80° ± 2° | Φ |
| 16 SKS, 10 SKS, 14 SKS | 2.1 ± 0.2 | 1.9 ± 0.1 | 1.3 ± 0.3 | $\delta t$ / s |
| Peru | | BAZ ~ 259° | | |
| SIMW | 90° ± 2° | 88° ± 1° | 165° ± 1° | Φ |
| 10 SKS, 10 SKS, 8 SKS | 1.9 ± 0.4 | 1.9 ± 0.3 | 1.9 ± 0.7 | $\delta t$ / s |
| Mexico | | BAZ ~ 295° | | |
| SIMW | 33° ± 1° | 34° ± 28° | 63° ± 12° | Φ |
| 14 SKS, 12 SKS, 10 SKS | 2.4 ± 0.5 | 0.9 ± 0.8 | 0.7 ± 0.1 | $\delta t$ / s |
| Solomon Islands | | BAZ ~ 39° | | |
| SIMW | 66° ± 16° | 36° ± 18° | 64° ± 9° | Φ |
| 1 SKKS, 3 SKKS, 1 SKKS | 1.2 ± 0.5 | 3.0 ± 1.5 | 1.2 ± 0.4 | $\delta t$ / s |

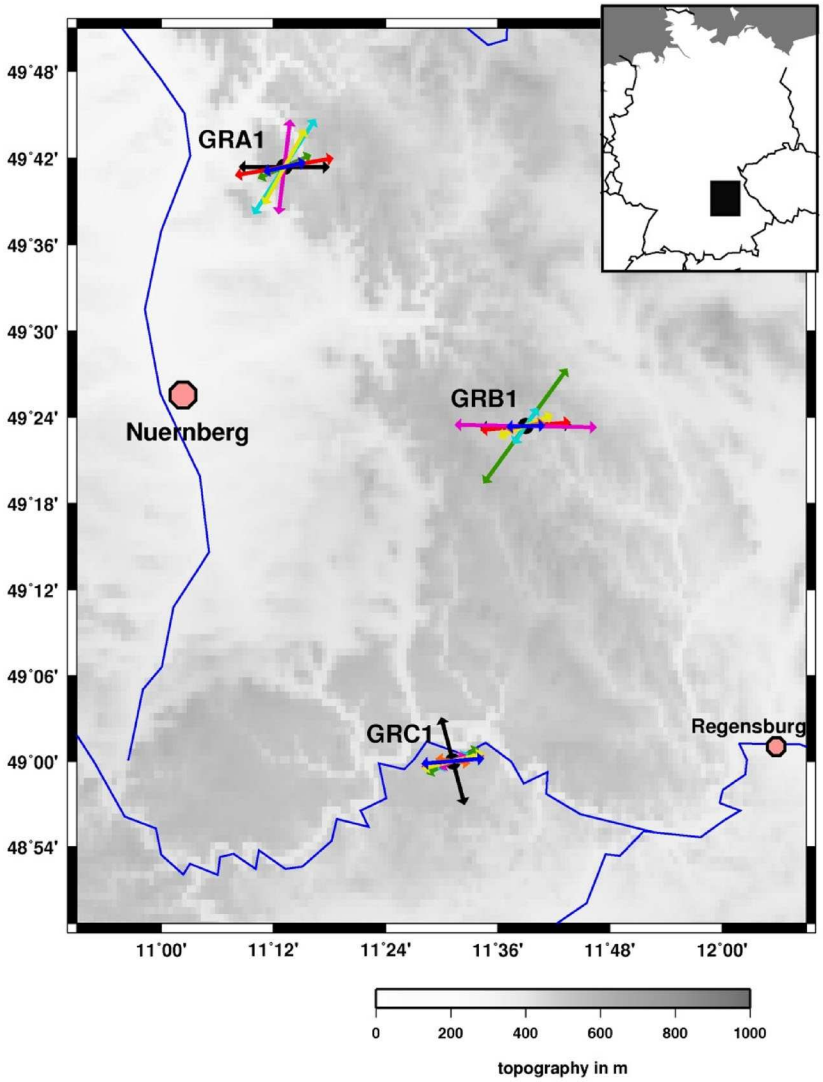


**Figure 9.** Splitting results (SIMW) at the GRF broadband seismic stations GRA1, GRB1 and GRC1, arrow direction is in direction of fast shear wave polarization, arrow length is proportional to delay time, and arrow colour corresponds to source region (see Fig. 1b).

3 s with a trend to lower values at GRC1 compared to GRA1 and GRB1 (Fig. 9). This variation in $\Phi$ and $\delta t$ is similar to recent results by Walther *et al*. (2014) as well as earlier results by Brechner *et al*. (1998) and partly by Plenefisch *et al*. (2001). In Table 3 the splitting results of the earlier studies are summarized. The reason for the variation of the splitting values between the three GRF stations is probably due to the transition between the Variscan, Moldanubian and Saxothuringian units in the region as discussed in Plenefisch *et al*. (2001).

In Fig. 10, $\Phi$ is shown as a function of backazimuth for the three recording stations GRA1 (red), GRB1 (green) and GRC1 (blue). The $\Phi$ values from SIMW are similar to the single measurements by Walther *et al*. (2014), but have narrower confidence boundaries (Fig. 11). The obtained $\Phi$ directions for station GRA1 (red) vary strongly, nearly periodical with backazimuth (Figs 10 and 11). Such a variation cannot be explained by a single layer with horizontally oriented anisotropy but requires a more complex anisotropic structure as explanation. Silver & Savage (1994) showed that, for example, two layers with differently horizontally oriented anisotropy could cause such backazimuth dependent splitting parameters as demonstrated in Fig. 12.

The results for station GRB1 (green in Figs 10 and 11b) do not vary strongly with backazimuth. Six of the eight $\Phi$ results are very close to their mean value of $84^\circ \pm 28^\circ$. The $\Phi$ results for the Solomon Islands (BAZ $\sim 39^\circ$, $\Phi \sim 36^\circ \pm 18^\circ$) and Mexico (BAZ $\sim 295^\circ$, $\Phi \sim 34^\circ \pm 28^\circ$) earthquake recordings differ from that mean value, possibly indicating a more complex structure underneath this station for waves arriving along these backazimuths. For the Solomon Islands sources the splitting parameters $\Phi$ and $\delta t$ have large error ranges (Fig. 10 and Table 2). Taking this into account, more results from different backazimuths are required to definitely precluding a single-layer model underneath station GRB1. Brechner *et al*. (1998) noted that the splitting parameters at GRB1 are complex and speculate about an inclined symmetry axis of the anisotropic structure.

All $\Phi$ values at station GRC1 (blue in Fig. 10) are close to their mean value of $75^\circ$, except for Peru earthquakes (BAZ $\sim 259^\circ$). For shear waves excited from earthquakes under Peru, the polarization

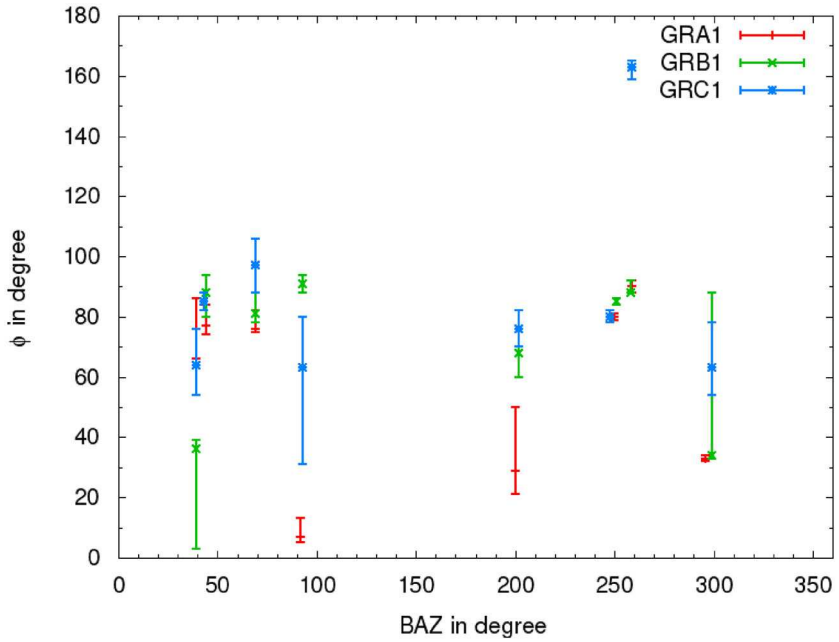


**Figure 10.** Fast polarization direction Φ and errors as function of backazimuth for the SIMW results at the three GRF stations.

**Table 3.** Anisotropy parameters in the vicinity of the Gräfenberg array. Sources: B73: Bamford (1973) using Pn phase travel times and the time-term method (tt). E96: Enderle *et al*. (1996) using Pn and tt plus petrophysical modelling to predict quasi shear wave velocities. V89c: Vinnik *et al*. (1989c) using SKS analysis. V94: Vinnik *et al*. (1994) using SKS analysis. B98: Brechner *et al*. (1998) using SKS splitting. F&V00: Fara & Vinnik (2000) using anisotropic *P*-wave receiver functions. P01: Plenefisch *et al*. (2001) using SKS splitting. W14: Walther *et al*. (2014) using SKS splitting, note that single layer models are preferred for GRB1 and GRC1, because two layer fitting is as good as one layer fitting.

| Source, method | GRA1 | GRB1 | GRC1 |
|---|---|---|---|
| B73, Pn, t-t | | $\Phi_{pn} = 20^\circ$ | |
| E96, Pn, t-t, petro mod. | | $\Phi_{pn} = 31^\circ$ $\Phi_{s,calc.} = 76^\circ$ | |
| V89c, SKS | | $\Phi = 90^\circ$ $\delta t = 0.7$ s | |
| V94 | $\Phi_u = 10^\circ$ $\delta t_u = 1.1$ s<br>$\Phi_l = 82^\circ$ $\delta t_l = 1.9$ s | Complex | Complex |
| B98, SKS | $\Phi_u = 40^\circ$ $\delta t_u = 1.15$ s<br>$\Phi_l = 115^\circ$ $\delta t_l = 1.95$ s | Complex | $\Phi_u = 85^\circ$ $\delta t_u = 1.45$ s<br>$\Phi_l = 50^\circ$ $\delta t_l = 0.35$ s |
| F&V00, aniso. RF | $\Phi_u = 20^\circ$ (31–80 km) *dvp/vp* = 0.05, *dvs/vs* = 0.03<br>$\Phi_l = 110^\circ$ (80–250 km) *dvp/vp* = 0.05, *dvs/vs* = 0.03 | | |
| P01, SKS | $\Phi \sim$ *E-W* | $\Phi \sim$ ESE-WNW | $\Phi \sim$ *E-W* |
| W14, SKS | $\Phi_u = 80^\circ$ $\delta t_u = 1.7$ s<br>$\Phi_l = 155^\circ$ $\delta t_l = 1.2$ s<br>Two layers | $\Phi_u = 85^\circ$ $\delta t_u = 1.0$ s<br>$\Phi_l = 80^\circ$ $\delta t_l = 0.5$ s<br>Single layer | $\Phi_u = 85^\circ$ $\delta t_u = 0.9$ s<br>$\Phi_l = 80^\circ$ $\delta t_l = 0.5$ s<br>Single layer |

direction of the radially polarized shear wave (equal to the BAZ) is close to the probable fast polarization direction under the station. Hence the obtained result can be either the actual fast polarization direction or the perpendicular direction (Wüstefeld & Bokelmann 2007). The latter would imply a Φ value of 75°, perfectly matching the other results. This independence of Φ from backazimuth implies that only a structure of a single anisotropic layer is required to explain the splitting parameters at GRC1. This is confirmed by the result of Walther *et al*. (2014), who find Φ = 80°–85° (Table 3) but no clear evidence for two separate layers.

The new splitting parameters Φ and $\delta t$ obtained with the SIMW method are compared with the recently published values of Walther *et al*. (2014) in Fig. 11. Their results were obtained by analysing single waveforms based on more than 20 yr of GRF data and represent the most comprehensive splitting parameter study for the Gräfenberg array at present. In general our SIMW results are consistent with the Walther *et al*. (2014) results for the backazimuth ranges of about 40° < BAZ < 80° and 240° < BAZ < 270°, that is, the source regions Japan, Molucca Sea, Chile and Peru. It is noticeable, however, that our SIMW results, especially for Φ, have considerably smaller error ranges. Furthermore, we were able to determine the splitting parameters for two additional backazimuth directions, which was not possible so far due to missing SKS recordings with high enough SNR (>3) for a splitting analysis with single records. Thus, we were able to improve the backazimuthal coverage with SIMW.

The BAZ-dependent behaviour of Φ and $\delta t$ allows us to resolve a two-layer model underneath station GRA1. In Fig. 12, we plot the theoretical Φ and $\delta t$ values for the two-layer model proposed by Walther *et al*. (2014): upper layer: $\Phi_u = 80^\circ$ and $\delta t_u = 1.7$ s,

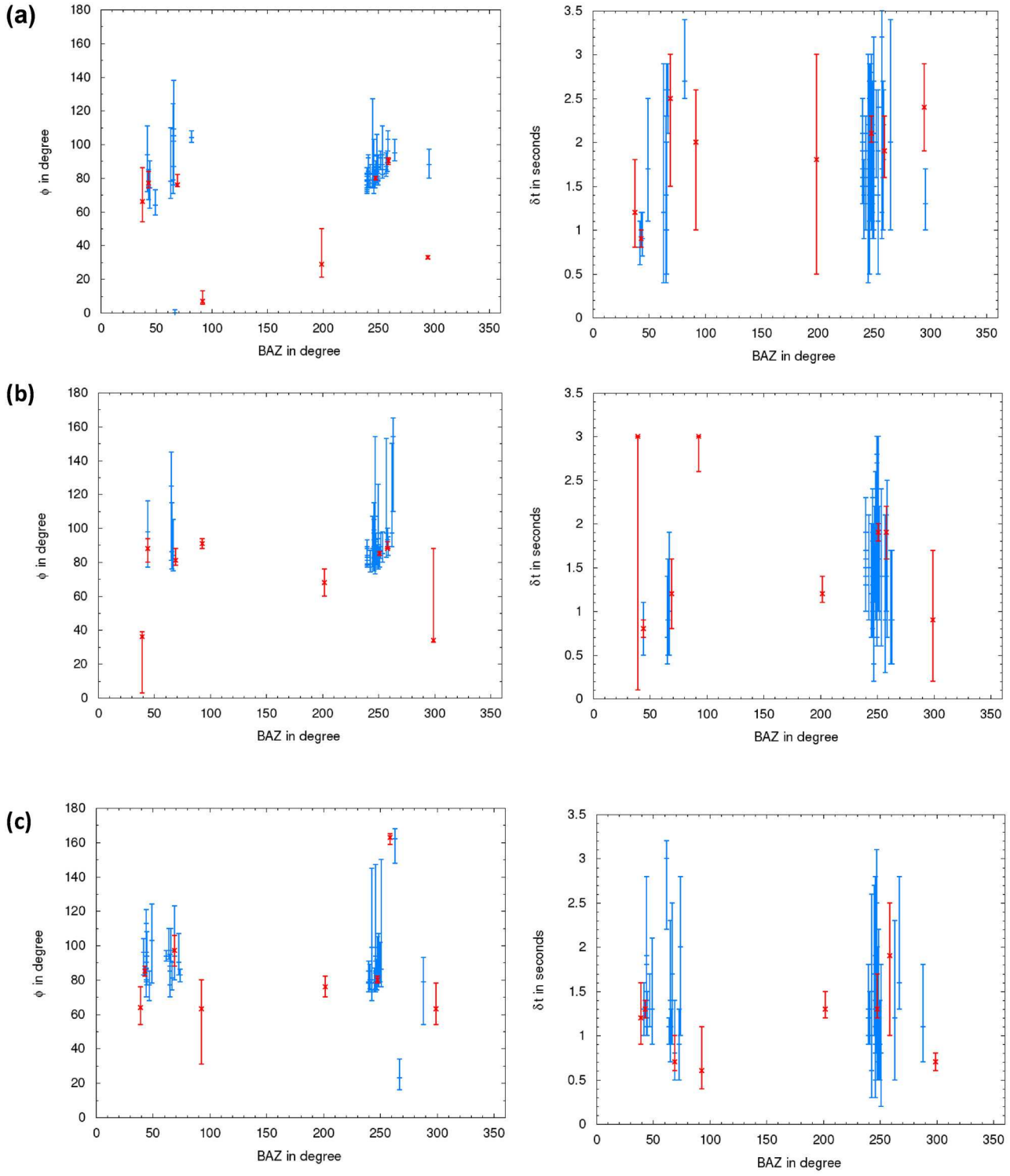


**Figure 11.** Fast polarization direction Φ and delay time $\delta t$ at the stations GRA1 (a), GRB1 (b) and GRC1 (c) as function of backazimuth. Comparison of our SIMW results (red) with results of single recordings from Walther *et al*. (2014) (blue).

lower layer: $\Phi_l = 155^\circ$ and $\delta t_l = 1.2$ s. This model can explain the observations very well including our additional new data points at BAZ $= 91^\circ$ (Sumatra earthquakes) and BAZ $= 199^\circ$ (South Sandwich Islands earthquakes). The merit of the new SIMW method is demonstrated by the fact that our results (red values in Fig. 12) match the model curves and confirm the anisotropic structure found by Walther *et al*. (2014) with more data points.

We also checked the limits of the possible model space as published by Walther *et al*. (2014) by using their extreme model values at the 95 per cent confidence limits and by calculating synthetic predictions for Φ as function of the backazimuth. Our new Φ values from SIMW in Figs 13(a) and (b) clearly do not fit for these extreme model boundaries. The preferred model in Fig. 12(a) fits much better, indicating that the average values Φ and $\delta t$ of Walther

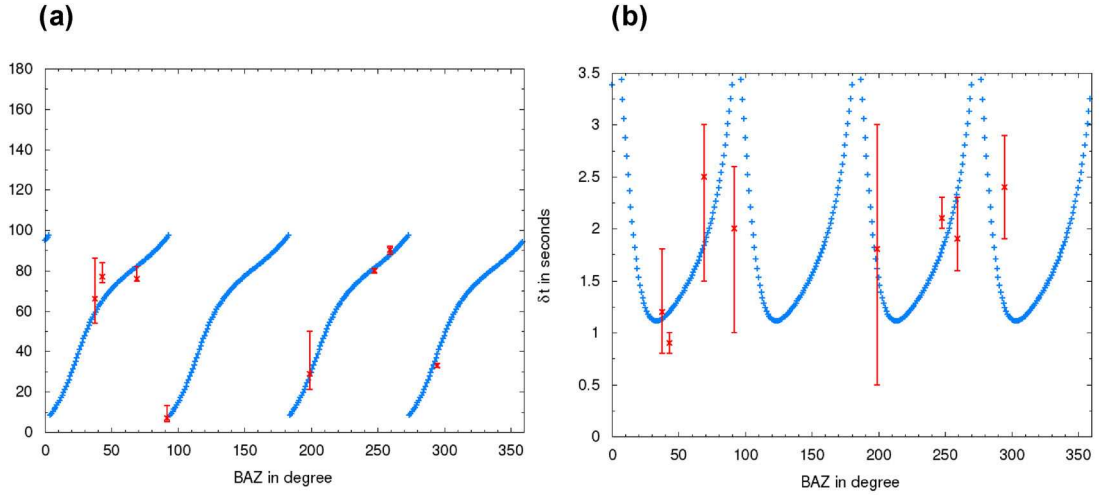


**Figure 12.** Theoretical behaviour of Φ (a) and $\delta t$ (b) for the two-layer anisotropy model of Walther *et al*. (2014) that is the best fit to their data: $\Phi_{\text{upper}} = 80^\circ$ and $\delta t_{\text{upper}} = 1.7$ s, $\Phi_{\text{lower}} = 155^\circ$ and $\delta t_{\text{lower}} = 1.2$ s (blue). Our SIMW results for GRA1 are plotted in red.

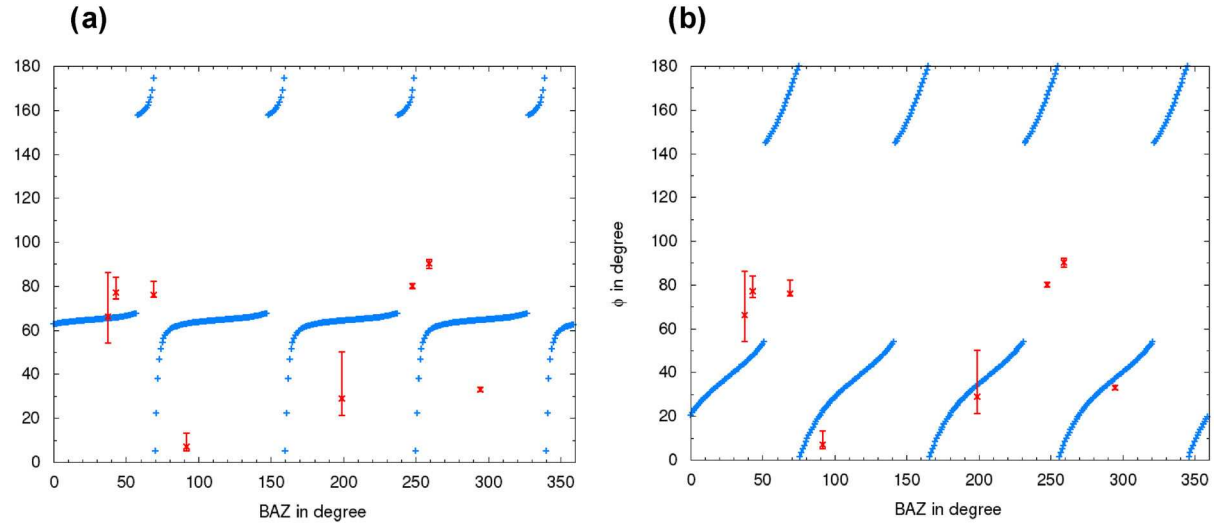


**Figure 13.** Our results for Φ (red) and the theoretical behaviour of Φ for two other two-layer anisotropy models (blue). Both input couples of $\Phi_{\text{upper}}/\Phi_{\text{lower}}$ lie at the edges of the 95 per cent confidence region of the inversion of Walther *et al*. (2014). (a) $\Phi_{\text{upper}} = 60^\circ$ and $\delta t_{\text{upper}} = 1.7$ s, and $\Phi_{\text{lower}} = 80^\circ$ and $\delta t_{\text{lower}} = 1.2$ s. (b) $\Phi_{\text{upper}} = 40^\circ$ and $\delta t_{\text{upper}} = 1.7$ s, and $\Phi_{\text{lower}} = 120^\circ$ and $\delta t_{\text{lower}} = 1.2$ s.

*et al*. (2014) are already well determined and that their uncertainty ranges may be overestimated.

Our model does not agree with some previous models (Table 3). Using anisotropic receiver function modelling, Farra & Vinnik (2000) determined a fast polarization direction of 20° between the Moho and 80 km depth and of 110° below. However, a spatial average is determined for the whole region below the Gräfenberg array, because waveforms are stacked across the stations GRA1, GRB1 and GRC1. In the uppermost mantle Bamford (1973) found a 20° direction as fast propagation direction of Pn phases. Later, Enderle *et al*. (1996) determined 31° for the fast propagation direction of Pn waves and they developed a petrophysical model, which was also fitted to Pn amplitudes and *P*-wave velocity-depth gradients. This petrophysical model predicted a fast shear wave polarization of 76° which is close to the value of 80°–85° by Walther *et al*. (2014) and our results. Such an offset in direction between the fast *P*-wave propagation direction and the fast shear wave polarization depends on the type of anisotropy and the 3-D alignment of the symmetry axes (Schulte-Pelkum & Blackman 2003). A new petrophysical model for the upper mantle underneath the Gräfenberg array is beyond the scope of this paper, but may be feasible soon when enough SKS recordings from the other 3-component stations, installed some years ago, are available.

## 5 CONCLUSIONS

The determination of the splitting parameters Φ and $\delta t$ with SKS and SKKS waves is often limited by the seismic background noise, which can strongly influence the splitting analysis. In order to improve the splitting analysis with recordings affected by low SNR, we propose to concatenate waveforms from similar events within a limited area of ±2° BAZ. Hence, the SKS signals and splitting properties are influenced along the same ray path. This processing procedure is similar to traditional waveform stacking, however, the characteristics of the single recordings are better preserved. The splitting parameters were then determined with the algorithm

of Silver & Chan (1991) by Simultaneous Inversion of Multiple Waveforms (SIMW).

The here presented algorithm is similar to the stacking methods proposed by Vinnik *et al*. (1989b) and Wolfe & Silver (1998). It can easily be show that these stacking methods and SIMW are linear processes and mathematically nearly equivalent. However, Vinnik *et al*. (1989b) and Wolfe & Silver (1998) stack the splitting results from different BAZ and incidence angles to obtain one stable set of splitting parameters for each station. With this approach all effects of azimuthally varying splitting observations are smeared out and the final result may be dominated by the observations from one BAZ.

Our first examples from NOA and GRF demonstrate that the SIMW method works well and provides stable results. As we use data from permanent arrays with carefully installed and maintained instruments, we assume that the seismometers are correctly oriented towards north and that there are no problems due to disorientations which may occur at other places (Tian *et al*. 2011).

Adding more waveforms during SIMW results in a convergence to stable results. As low SNR waveforms can be used, it is possible to determine $\Phi$ and $\delta t$ for backazimuths that would otherwise not be observable. These additional backazimuths are essential to estimate better anisotropy models for further geodynamic interpretation, especially in regions with inclined or multiple anisotropic layers. For both, NOA and GRF, $\Phi$ and $\delta t$ are calculated for backazimuths, which were not observed before. For NOA, a more complicated distribution of fast polarization directions is found, which needs further modelling and observations for a consistent explanation. The situation at GRF seems to be less complicated with a two-layer anisotropic model at station GRA1 in the northern part and a one-layer anisotropic model in the south (GRC1).

Following these first results with the proposed SIMW algorithm, we recommend to apply it also for data at other stations, especially at temporarily installed broadband stations. Their recordings are often influenced by higher noise amplitudes compared to permanent stations and their short recording times allow often only the analysis of low magnitude earthquakes. Such datasets will benefit from the SIMW method in the future.

## ACKNOWLEDGEMENTS

CR's stay at NORSAR was supported with a NERA project grant (EC project number 262330). The waveforms were provided by NORSAR and Bundesanstalt für Geowissenschaften und Rohstoffe, Hannover. Plotting was done with GMT (Wessel & Smith 1998). We thank two anonymous reviewers for helping improving the manuscript. This is Berkeley contribution # 2016-6.

## REFERENCES

Bamford, D., 1973. Refraction data in Western Germany – a time-term interpretation, *Z. Geophys.,* **39,** 907–927.

Brechner, S., Klinge, K., Krüger, F. & Plenefisch, T., 1998. Backazimuthal variations of splitting parameters of teleseismic SKS phases observed at the broadband stations in Germany, *Pure appl. Geophys.,* **151,** 305–331.

Enderle, U., Mechie, J., Sobolev, S. & Fuchs, K., 1996. Seismic anisotropy within the uppermost mantle of southern Germany, *Geophys. J. Int.,* **125,** 747–767.

Farra, V. & Vinnik, L., 2000. Upper mantle stratification by P and S receiver functions, *Geophys. J. Int.,* **141,** 699–712.

Gledhill, K. & Gubbins, D., 1996. SKS splitting and the seismic anisotropy of the mantle beneath the Hikurangi subduction zone, New Zealand, *Phys. Earth planet. Inter.,* **95,** 227–236.

Green, P.E., Jr., Kelly, E.J., Jr. & Levin, M.J., 1966. A comparison of seismic array processing methods, *Geophys. J. R. astr. Soc.,* **11,** 67–84.

Harjes, H-P. & Seidl, D., 1978. Digital recording and analysis of broadband seismic data at the Gräfenberg (GRF)-Array, *J. Geophys.,* **44,** 511–523.

Kind, R., Kosarev, G. L., Makeyeva, L.I. & Vinnik, L.P., 1985. Observations of laterally inhomogenous anisotropy in the continental lithosphere, *Nature,* **318,** 358–361.

Krüger, F., Weber, M., Scherbaum, M. & Schlittenhardt, J., 1993. Double beam analysis of anomalies in the core-mantle boundary region, *Geophys. Res. Lett.,* **20,** 1475–1478.

Long, M.D. & Becker, T., 2010. Mantle dynamics and seismic anisotropy, *Earth planet. Sci. Lett.,* **297,** 341–354.

Long, M.D. & van der Hilst, R.D., 2005. Estimating shear-wave splitting parameters from broadband recordings in Japan: a comparison of three methods, *Bull. seism. Soc. Am.,* **95,** 1346–1358.

Nicolas, A. & Christensen, N.I., 1987. Formation of anisotropy in upper mantle peridotites—a review, in *Composition, Structure and Dynamics of the Lithosphere–Asthenosphere System,* pp. 111–123, eds Fuchs, K. & Froidevaux, C., Geodyn. Ser., 16. American Geophysical Union.

Plenefisch, T., Klinge, K. & Kind, R., 2001. Upper mantle anisotropy at the transition zone of the Saxothuringicum and Moldanubicum in southeastern Germany revealed by shear wave splitting, *Geophys. J. Int.,* **144,** 309–319.

Ribe, N.M. & Yu, Y., 1991. A theory for plastic deformation and textural evolution of olivine polycrystals, *J. geophys. Res.,* **96,** 8325–8335.

Roy, C. & Ritter, J.R.R., 2013. Complex deep seismic anisotropy below the Scandinavian Mountains, *J. Seismol.,* **17,** 361–384.

Savage, M.K., 1999. Seismic anisotropy and mantle deformation: what have we learned from shear wave splitting?, *Rev. Geophys.,* **37,** 65–106.

Schulte-Pelkum, V. & Blackman, D.K., 2003. A synthesis of seismic P and S anisotropy, *Geophys. J. Int.,* **154,** 166–178.

Schweitzer, J., Fyen, J., Mykkeltveit, S., Gibbons, S.J., Pirli, M., Kühn, D. & Kværna, T., 2012. Seismic arrays, in *New Manual of Seismological Observatory Practice (NMSOP-2),* 2nd (revised) edn, 80 pp, ed. Bormann, P., Deutsches GeoForschungsZentrum GFZ, http://ebooks.gfz-potsdam.de/pubman/item/escidoc:43213:7, doi: 10.2312/GFZ.NMSOP-2_ch9.

Silver, P.G. & Chan, W.W., 1991. Shear wave splitting and subcontinental mantle deformation, *J. geophys. Res.,* **96,** 16 429–16 454.

Silver, P.G. & Savage, M.K., 1994. The interpretation of shear-wave splitting parameters in the presence of two anisotropic layers, *Geophys. J. Int.,* **119**(3), 949–963.

Silver, P.G. & Chan, W.W., 1988. Implications for continental structure and evolution from seismic anisotropy, *Nature,* **355,** 34–39.

Tian, X., Zhang, J., Si, S., Wang, J., Chen, Y. & Zhang, Z., 2011. SKS splitting measurements with horizontal component misalignment, *Geophys. J. Int.,* **185,** 329–340.

Vecsey, L., Plomerová, J. & Babuška, V., 2008. Shear-wave splitting measurements – Problems and solutions, *Tectonophysics,* **462,** 178–196.

Vinnik, L.P., Farra, V. & Romanowicz, B., 1989a. Observational evidence for diffracted SV in the shadow of the Earth's core, *Geophys. Res. Lett.,* **16,** 519–522.

Vinnik, L.P., Farra, V. & Romanowicz, B., 1989b. Azimuthal anisotropy in the Earth from observations of SKS at Geosope and NARS broadband stations, *Bull. seism. Soc. Am.,* **79,** 1543–1558.

Vinnik, L.P., Kosarev, G.L. & Makeyeva, L.I., 1984. Lithosphere anisotropy from the observation of SKS and SKKS waves, *Doklady Akademii Nauk SSSR,* **278,** 1335–1339.

Vinnik, L.P., Kind, R., Kosarev, G.L. & Makayeva, L.I., 1989c. Azimuthal anisotropy in the lithosphere from observations of long-period *S*-waves, *Geophys. J. Int.,* **99,** 549–559.

Vinnik, L.P., Krishna, V.G., Kind, R., Bormann, P. & Stammler, K., 1994. Shear wave splitting in the records of the German Regional Seismic Network, *Geophys. Res. Lett.,* **21**(6), 457–460.

Walther, M., Plenefisch, T. & Ruempker, G., 2014. Automated analysis of SKS splitting to infer upper mantle anisotropy beneath Germany using more than 20 yr of GRSN and GRF data, *Geophys. J. Int.,* **196,** 1207–1236.

Wessel, P. & Smith, W.H.F., 1998. New, improved version of Generic Mapping Tools released, *EOS, Trans. Am. geophys. Un.,* **79,** 579.

Wolfe, C. & Silver, P. G., 1998. Seismic anisotropy of oceanic upper mantle: Shear wave splitting methodologies and observations, *J. geophys. Res.,* **103,** 749–771.

Wüstefeld, A. & Bokelmann, G., 2007. Null detection in shear-wave splitting measurements, *Bull. seism. Soc. Am.,* **97**(4), 1204–1211.

Wüstefeld, A., Bokelmann, G., Zaroli, C. & Barruol, G., 2008. SplitLab: A shear-wave splitting environment in Matlab, *Comput. Geosci.,* **34**(5), 515–528.

Yu, W. & Wen, L., 2012. Deep-focus repeating earthquakes in the Tonga–Fiji subduction zone, *Bull. seism. Soc. Am.,* **102,** 1829–1849.